Soft Matter

Accepted Manuscript

ROYAL SOCIETY OF CHEMISTRY

www.rsc.org/softmatter

The role of acrylonitrile in controlling the structure and properties of nanostructured ionomer films

Somjit Tungchaiwattana, Muhamad Sharan Musa, Junfeng Yan, Peter A. Lovell, Peter Shaw and Brian R. Saunders*

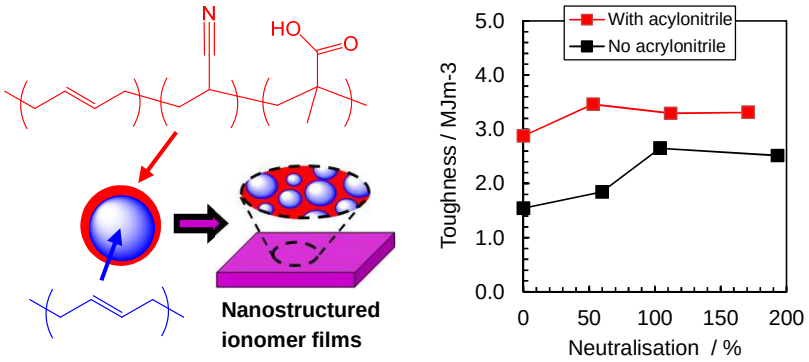

Copolymerisation of acrylonitrile within core-shell nanoparticles gives ductile nanostructured ionomer films with increased modulus values

1

The role of acrylonitrile in controlling the structure and properties of nanostructured ionomer films

Somjit Tungchaiwattana[a], Muhamad Sharan Musa[a], Junfeng Yan[a], Peter A. Lovell[a], Peter Shaw[b] and Brian R. Saunders[a,*]

[a]*Polymer Science and Technology Group, The School of Materials, The University of Manchester, Grosvenor Street, M13 9PL, UK.* [b]*Synthomer Ltd, Temple Fields, Harlow, Essex, CM20 2BH, U.K.*

ABSTRACT

Ionomers are polymers which contain ionic groups that are covalently bound to the main chain. The presence of a small percentage of ionic groups strongly affects the polymer's mechanical properties. Here, we examine a new family of nanostructured ionomer films prepared from core-shell polymer nanoparticles containing acrylonitrile (AN), 1,3-butadiene (Bd) and methacrylic acid (MAA). Three new AN-containing dispersions were investigated in this study. The core-shell nanoparticles contained a PBd core. The shells contained copolymerised Bd, AN and MAA, i.e., PBd-AN-MAA. Three types of crosslinking were present in these films: covalent crosslinks (from Bd); strong physical crosslinks (involving ionic bonding of $RCOO^-$ and Zn^{2+}) and weaker physical crosslinks (from AN). We examined and compared the roles of AN and ionic crosslinking (from added Zn^{2+}) on the structure and mechanical properties of the films. The FTIR spectroscopy data showed evidence for RCOOH-nitrile hydrogen bonding with tetrahedral geometry. DMTA studies showed that AN copolymerised within the PBd-AN-MAA phase uniformly. Tensile stress-strain data showed that inclusion of AN increased elasticity and toughness. Analysis showed that about 33 AN groups were required to provide an elastically-effective chain. However, only 1.5 to 2 ionically bonded $RCOO^-$ groups were required to generate an elastically-effective chain. By contrast to ionic bonding, AN inclusion increased the modulus without compromising ductility. Our results show that AN is an attractive, versatile, monomer for increasing the toughness of nanostructured ionomers and this should also be the case for other nanostructured polymer elastomers.

INTRODUCTION

Nanostructured particles[1-4] and materials[5] have attracted a great deal of interest in the literature. Ionomers are polymers containing a minor fraction of ionic groups that are typically covalently bonded to the polymer chain backbone as pendant species[6]. The mechanical properties of ionomers can be greatly improved by the presence of a small ionic group concentration (< 10 mol.%). The seminal studies by Eisenberg et al. established a clear mechanistic explanation for this mechanical property enhancement[7]. Ionic aggregates were found to act as reversible crosslinks and their effectiveness was dependent on the nature of the polymer and ionic groups. Because of their favourable mechanical properties there has been much interest in ionomers as thermoplastic elastomers and an example commercial material is Surlyn[8]. Ionomers have also attracted considerable interest for application in polymer electrolyte fuel cells[9, 10]. The continuing interest in ionomers is evidenced by their increasing architectural complexity which has resulted in well-defined ionomers with tuneable properties[11, 12]. Ionomer examples now include biodegradable ionomers[13, 14], shape-memory ionomers[15], self-healing ionomers[16], ionomer/clay nanocomposites[17] and ionomers with pendant vinyl groups that can be subsequently covalently crosslinked[18]. An emerging theme involves preparing precisely sequenced ionomers with well-defined spacing between the ionic groups[19]. We have approached nanostructuring of ionomers in a different way by studying ionomers prepared from ionic core-shell elastomeric polymer nanoparticles[20, 21]. Unlike conventional ionomers[12], our nanostructured ionomer films are prepared by deposition from aqueous dispersions and the RCOOH groups are neutralised using Zn^{2+}. The latter is supplied from dispersed ZnO particles. Our previous nanostructured ionomers were based exclusively on poly(butadiene) (PBd) and methacrylic acid (MAA). Acrylonitrile (AN) is known to increase the elasticity of copolymers[22]. Here, we examine the effects of including copolymerised AN on the structure and mechanical properties of deposited nanostructured PBd-based ionomer films. We investigate the hypothesis that AN should cause an increase in elasticity due to the increased

stiffness associated with AN segments. We also compare the roles of AN and neutralisation in determining the mechanical properties of the nanostructured films.

PAN is a polar polymer that shows crystalline order[22]. PAN has very high modulus values of up to 35 GPa for drawn fibers[23]. The polymer has strong intermolecular interactions[24] and the chains have low segment mobility due to the high dipole-dipole attraction between neighbouring nitrile groups[25, 26]. PAN has a high tendency to crystallise, even in the atactic form[27]. Dufour et al.[28] studied three-arm block copolymer thermoplastic elastomers containing poly(butylacrylate) and PAN. Glassy PAN microdomains formed which acted as physical crosslinks and increased the elastic modulus. The versatility of AN to provide polymers with interesting properties has also recently been shown in the context of copolymers with upper critical solution temperatures[29]. Here, we incorporated AN in the shells of core-shell nanoparticles (Scheme 1(a)) and then used those dispersions to form nanostructured ionomer films (Scheme 1(b)). The films are composed of interlinked core-shell nanoparticles and are nanostructured at the colloidal scale with ionic crosslinking being provided by Zn^{2+}. The latter was supplied by dispersed ZnO particles. Our ionomers are prepared by an aqueous dispersion mixing and casting approach (Scheme 1(b)) and are therefore environmentally friendly. They differ considerably from conventional ionomers which are usually prepared from non-aqueous polymer solutions or melts using casting methods[30, 31]. It was envisaged that the AN chain segments would act as local, non-permanent, physical crosslinks and increase the modulus and this hypothesis was investigated. The novelty of the present study compared to our earlier report[21] resides in the inclusion of AN and the elucidation the role of AN in governing the mechanical properties of nanostructured ionomer films. This study introduces three new nanoparticle dispersions and nanostructured films, all of which contain AN.

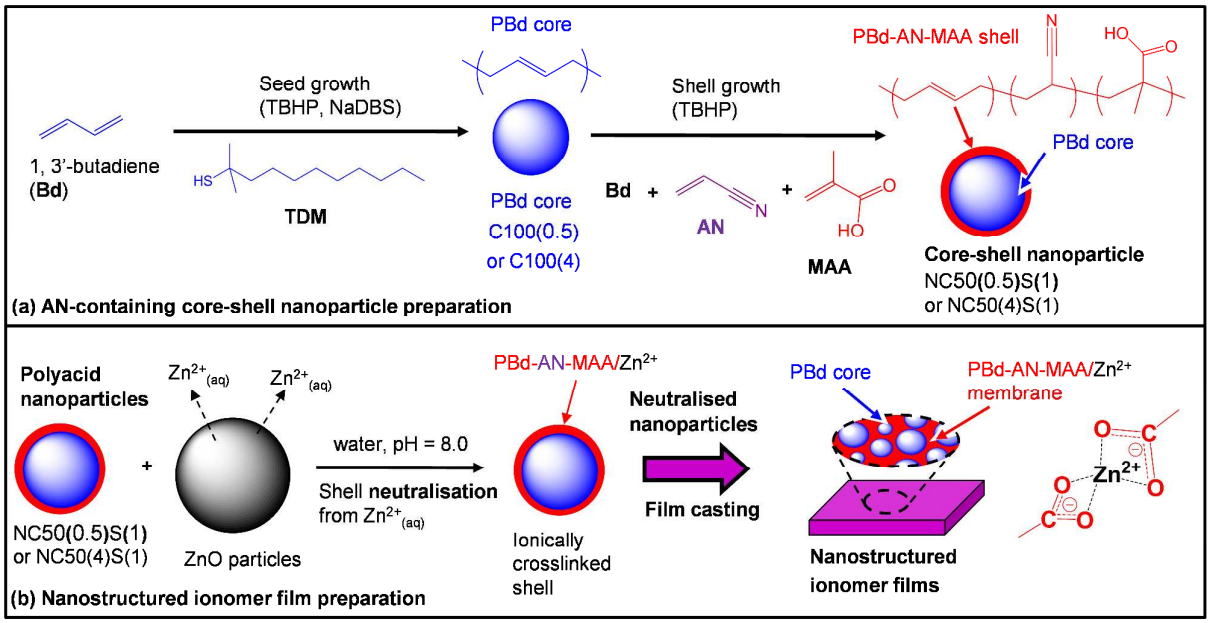

Scheme 1. (a) depicts the preparation of core-shell AN-containing nanoparticles by seeded, starved-feed emulsion polymerisation. (b) shows the formation of nanostructured films by dispersion casting onto a glass substrate using mixed nanoparticle / ZnO dispersions. TDM, NaDBS and TBHP are *tert*-dodecylmercaptan, sodium dodecylbenzene sulfonate and *tert*-butyl hydroperoxide, respectively.

The study begins with characterisation of the core-shell nanoparticles. The data are discussed and also compared to one AN-free model system from our earlier work[21]. This comparison is very useful because it enables the role of AN in determining the film properties to be elucidated. The spectroscopic and structural properties of the nanostructured ionomer films are then investigated. The mechanical properties of these films were probed using dynamic mechanical thermal analysis (DMTA) and stress-strain measurements. We conclude with a discussion of the structure-property relationships for the new AN-containing nanostructured ionomer films. A key outcome for this study is that AN is found to increase the modulus without compromising ductility, which is contrary to the behaviour normally observed for elastomers.

EXPERIMENTAL

Reagents and nanoparticle preparation

The monomers used in this study as well as the other chemicals for emulsion polymerisation were provided by Synthomer Ltd and used as received. The key difference between the nanoparticles used here and our previous work[20, 21] is the inclusion of AN as described below. The ZnO dispersion used

for neutralisation was purchased from Aquaspersions Ltd, UK and had an average size of 2 μm. The methods for nanoparticle preparation and film preparation were the same as those described in detail earlier[21]. The difference to the previous work is that AN was included in the co-monomer feeds used to prepare the nanoparticle shells. Briefly, the core-shell nanoparticles were prepared by seeded, starved-feed emulsion copolymerisation using PBd seed nanoparticles. The codes used for the seeds are C100(0.5) and C100(4), which indicates that these PBd nanoparticles were prepared using 0.5 or 4.0 wt.% *tert*-dodecylmercaptan (TDM) with respect to monomer. Those nanoparticle seeds were the same as those used in the earlier study[21]. Copolymer shells were grown from the seeds at 60 ^{o}C. The initiator was *t*-butyl hydroperoxide (TBHP) and the surfactant was sodium dodecylbenzene sulfonate (NaDBS). The nanoparticle concentration of the as-made latexes was about 35 w/w%. Further details are given in Table 1. The code NC50(0.5)S(1) represents PBd/PBd-AN-MAA nanoparticles where the core (PBd) and shell (PBd-AN-MAA) both had nominal concentrations of 50 wt.% based on the masses of monomers and seed used during their preparation. The TDM concentrations used for the core and shell were 0.5 and 1.0 w/w% with respect to total monomer. In this case the core nanoparticles were C100(0.5) (Table 1). NS100(1) was a uniform (non-core-shell) system that did not contain a seed. NS100 was prepared via batch emulsion copolymerisation using monomer-flooded conditions. Data for the AN-free C50(0.5)S(1) nanoparticles and film are from the earlier study[21] and are used for comparison to help elucidate the role of AN in governing mechanical properties.

Table: 1 Compositions of the core-shell nanoparticles used to prepare nanostructured ionomer films

Code	Core/shell[a]	C_{TDM} [b] / (wt.%)	$W_{AN(Tot)}$ [c]	$W_{MAA(Tot)}$ [d]	pK_a [e]	D_{TEM} [f] / nm	d_h [g] / nm	δ_{TEM} [h] /nm
NC50(0.5)S(1)	PBd/PBd-AN-MAA	0.50	12.5	3.30	9.55	66 (38)	100	3
NC50(4)S(1)	PBd/PBd-AN-MAA	4.0	12.5	3.25	9.45	73 (37)	103	8
NS100S(1)	PBd-AN-MAA	1.0	25.0	6.30	9.70	79 (15)	84	-
C50(0.5)S(1)[i]	PBd/PBd-MAA	0.50	0	2.90	9.15	73 (27)	-	7
C100(0.5)	PBd	0.50	0	-	-	60 (37)	96	-
C100(4)	PBd	1.0	0	-	-	57 (41)	102	-

[a] The core-shell systems contained a nominal core volume fraction of 50 vol.% [b]TDM concentration used to prepare the seed (core) or whole nanoparticles. [c] Overall nominal AN concentration (wt.%) in the nanoparticle assuming 100% conversion. [d] Overall concentration of MAA (wt.%) in the nanoparticles based on titration data. [e] Apparent pK_a values determined from titration data. [f]Number-average nanoparticle size measured using TEM. The number in brackets is the coefficient of variation (= 100 x standard deviation / mean). [g] Hydrodynamic diameter. [h] Shell thicknesses estimated from TEM data using $(D_{TEM(cs)} - D_{TEM(c)})/2$, where $D_{TEM(cs)}$ and $D_{TEM(c)}$ are the diameters for the core-shell nanoparticles and core nanoparticles (e.g., C100(0.5) or C100(4)), respectively. [i] From Ref. 21.

Nanostructured ionomer film preparation

The nanocomposite films were prepared using the same procedure described fully earlier[21]. Briefly, the films were prepared by casting the aqueous dispersions onto glass plates in a temperature and humidity controlled room and dried at 25 ^{o}C for 1 day. The dried films had thicknesses in the range of 200 – 400 μm. Some films were prepared from nanoparticle dispersions without any pH adjustment. The initial dispersion pH was about 5 and those films are termed polyacid films. Films neutralised with Zn^{2+} were prepared by adding the appropriate mass of ZnO particle dispersion (~ 56 wt.%) to the core-shell nanoparticle dispersion (which had been diluted to 30 wt.% in water) for which the pH had been pre-adjusted to 8.0 using aqueous KOH solution. The extent of neutralisation used in this study is the nominal value (α_{nom}). The value of α_{nom} represents the molar ratio of the cationic charge added to the number of moles of RCOOH groups initially present. Values of α_{nom} = 0 and 100% correspond to films that were in the polyacid and fully neutralised states, respectively. Values of α_{nom} greater than 100% imply that excess ZnO was present. The Zn^{2+} and K^{+} cations both contribute to neutralisation[21] and originate from ZnO and KOH, respectively. The RCOOH concentration within the nanoparticles was determined from titration data (Table 1).

Physical Measurements

The hydrodynamic diameters (d_h) of the nanoparticles were measured using a Brookhaven Instrument Corporation BI-9000 correlator with a Brookhaven BI-200SM goniometer using an angle of 90°. The samples were irradiated using a Spectra Physics 20 mW HeNe laser (632.8 nm). The d_h values obtained from the latter were z-average values calculated using cumulant analysis. TEM measurements were conducted using a Philips CM 30 instrument. The samples were subjected to negative staining using phosphotungstic acid solution (2 wt.%). The nanoparticles were deposited on Holey carbon grids (Agar Scientific Ltd). More than 100 nanoparticles were counted to determine the number-average nanoparticle size (D_{TEM}). Titration data were obtained using a Mettler DL53 autotitrator. ATR FTIR data were obtained using a Nicolet 5700 FTIR instrument using cast films and a resolution of 1 cm^{-1}. DMTA data were measured using a TA-Q800 instrument and the tensile mode (1 Hz). A Dimension 3100 AFM (Digital Instruments, Santa Barbara, CA) operated in tapping mode was used to map the surface morphology of thin films at ambient conditions. Tensile tests were performed using a Hounsfield H10KS-0079 tensile testing instrument. The measurements were performed at 25 °C at 50% RH. Samples were prepared as dumbbell shapes. The overall length was 75 mm and the constricted width was 4.0 mm. The length of the constricted region was 30 mm. The extension rate was 500 mm / min. Wide-angle X-ray diffraction (WAXD) experiments were conducted using a Philips X'pert Modular Powder Diffractometer (MPD) at room temperature. The generator setting (40 mA, 45 kV) was used to produce monochromatic X-rays, anode Cu Kα radiation of wavelength 1.542Å. The dimensions of the film specimens used for testing was 40 mm x 40 mm x 0.20 mm.

RESULTS

Nanoparticle characterisation

A seeded, starved-feed method was used to prepare the core-shell nanoparticles used in this study (Table 1). The core-shell nature of the AN-free C50(0.5)S(1) nanoparticles (which are used here for

comparison) was established conclusively in two earlier studies[20, 21]. The AN-containing system (NC50(0.5)S(1)) and C50(0.5)S(1) were prepared using the same seed (C100(0.5)). The inclusion of minor proportions of AN during the shell growth of the new NC50(0.5)S(1) and NC50(4)S(1) nanoparticles studied here is highly unlikely to have prevented shell formation. The evidence presented in this study points to copolymerisation of Bd and AN within the shells of the NC50(0.5)S(1) and NC50(4)S(1) nanoparticles.

TEM images of all of the nanoparticles considered in this study are shown in Fig. S1. Histrograms for the size distributions are also shown in Fig. S1. The nanoparticles were generally spherical although some were deformed due to their glass transition temperatures being well below room temperature. Data for the AN-free system from the earlier study[21] (C50(0.5)S(1)) are included for comparison with NC50(0.5)(1). As a further comparator, an AN-containing non-core shell system (NS100(1)) was prepared and investigated for this study.

The number-average diameters determined from TEM were in the range of 66 to 79 nm and were used to estimate approximate shell thicknesses (δ_{TEM}, Table 1). The δ_{TEM} values are consistent with core-shell morphologies. The hydrodynamic diameters for the nanoparticles (Table 1) are all larger than those determined by TEM, as expected. The nanoparticles had significant size polydispersities as judged by the coefficients of variation (Table 1). The high polydispersities originated from the PBd nanoparticle seeds and, as was previously noted[20, 21], do not prevent useful structure-property relationships from being discerned.

The apparent pK_a values (Table 1) from potentiometric data (Fig. S2) were in the range of 9.1 to 9.7 and are much higher than that reported for PMAA (ca. 6.0[32]). This trend has been noted earlier for PBd-MAA nanoparticles[32] and is ascribed to the low dielectric constant of the present nanoparticles. The implications of a high pK_a values are that neutralisation of the polyacid nanoparticles prior to film formation (which occurred at pH = 8) was conducted under conditions where a high proportion

of RCOOH was present. The RCOOH groups were converted into ionically crosslinked $RCOO^-$ groups during the neutralisation process by reaction with Zn^{2+} that was dissolved in the aqueous phase and provided by the dispersed ZnO particles.

Nanoparticle film ionic bonding, structure and morphology

Nanostructured films were prepared using an aqueous dispersion casting method. We first consider films prepared without any pH adjustment or added ZnO. Those polyacid (non-neutralised) nanostructured films were cast from dispersions with pH values of about 5. FTIR spectra for the films are shown in Fig. 1. The nitrile band (C≡N) was present for the AN-containing systems (Fig. 1(a)) at 2237 cm^{-1} and is similar to that reported for other AN-based co-polymers[33, 34]. (Of course the band was absent for C100(0.5)S(1).) The FTIR spectra confirm that successful copolymerisation of AN occurred within NC50(0.5)S(1), NC50(0.5)S(4) and NS100(1) nanoparticles.

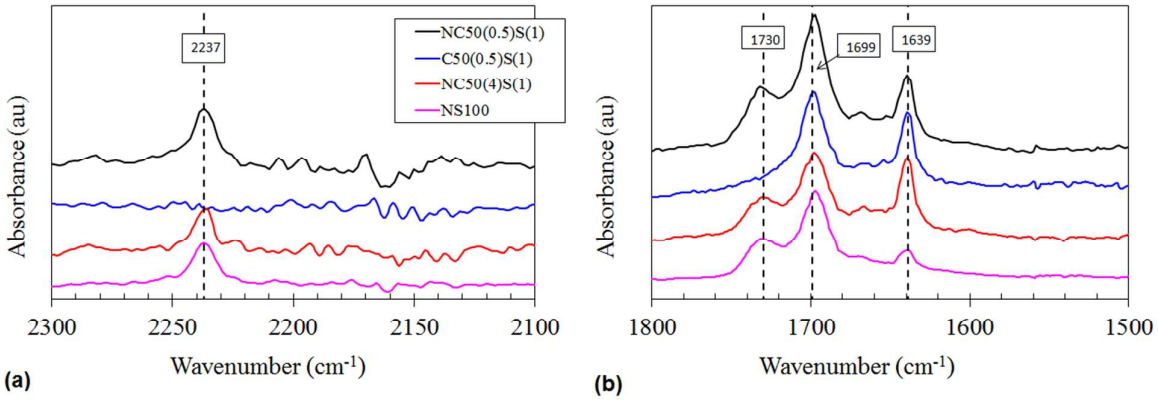

Fig. 1 FTIR spectra for various polyacid nanostructured films (α_{nom} = 0%). The legend applies to both figures.

The spectra from Fig. 1(b) show the region containing RCOOH bands. Bands are evident at 1699 and 1639 cm^{-1} due to dimeric H-bonded RCOOH[35] and C=C[36], respectively. Interestingly, the spectra for the AN-containing films had a new, unique, band at 1730 cm^{-1}. This band was *absent* in the spectrum for C50(0.5)S(1) which shows that it must involve AN. Moreover, the reported IR spectrum of PAN[33] did not show a band in this position. We therefore ascribe the new 1730 cm^{-1} band to a stretching frequency involving CN groups. PMAA which is H-bonded to ether oxygen

atoms of poly(vinylmethylether) has a band at[37] 1730 cm^{-1}. By analogy with the latter, it is proposed that the 1730 cm^{-1} band is due to RCOOH groups H-bonded to the nitrogen of the C≡N group.

The effect of neutralisation on the FTIR spectra for the films was also studied (Fig. 2). It can be seen from Fig. 2(a) that the absorbance of the band at 1699 cm^{-1} decreased with increasing neutralisation (α_{nom}). This trend can also be seen for the C50(0.5)S(1) films and was reported earlier[21]. Importantly, for the present study the intensity of new band at 1730 cm^{-1} *also* decreased with increasing α_{nom}. This supports our proposal that the 1730 cm^{-1} band involved H-bonded RCOOH groups. As the extent of neutralisation increased a new band emerged at ~ 1588 cm^{-1} which is ascribed to[36, 38, 39] formation of tetrahedral binding $(Zn^{2+})(RCOO^{-})_2$ ionic complex. The same band was present for the C50(0.5)S(1) films (Fig. 2(c)) which did not contain AN. The position of this band was not affected by AN. It follows that *two* H-bonded RCOOH environments within the polyacid AN-containing films (dimeric RCOOH and AN-RCOOH) were converted to *one* single ionic environment ($(Zn^{2+})(RCOO^{-})_2$) upon neutralisation.

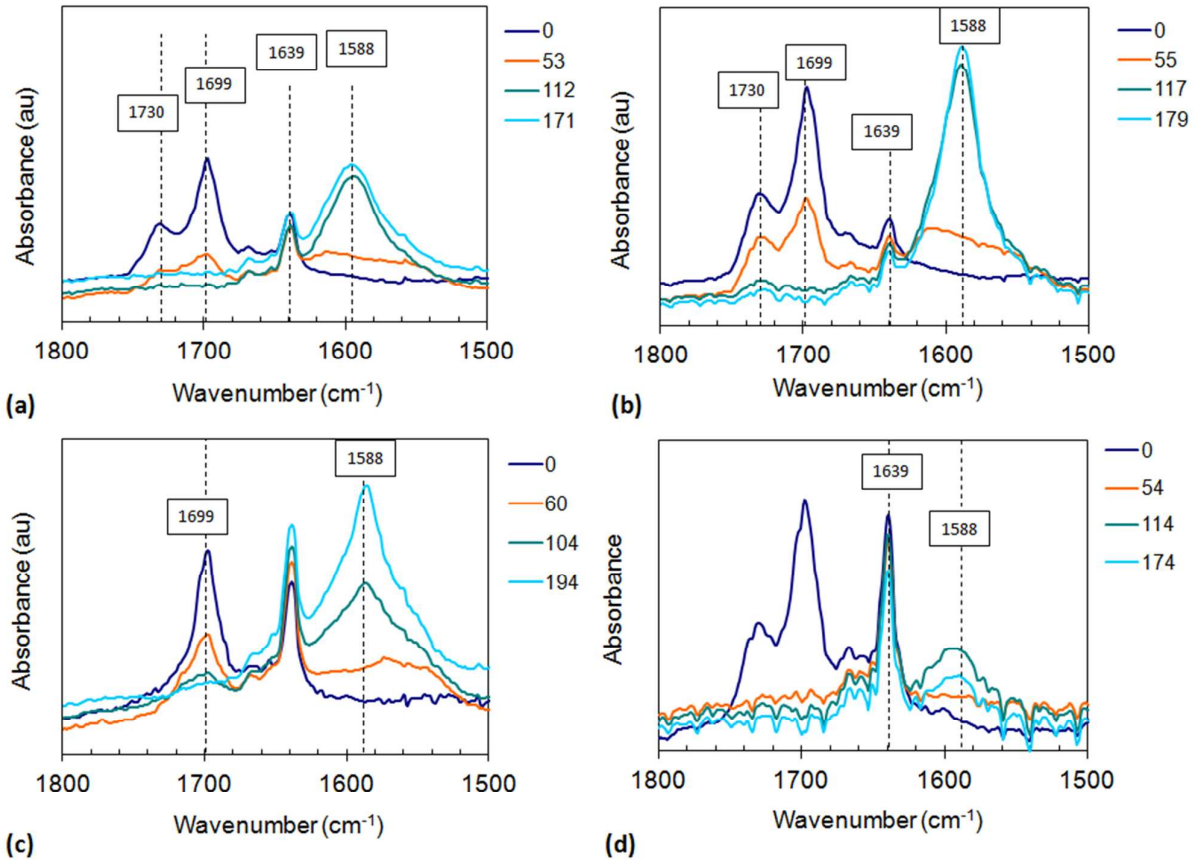

Fig. 2. FTIR spectra of (a) NC50(0.5)S(1), (b) NS100(1) (c) C50(0.5)S(1) and (d) NC50(4)S(1) films at different extents of neutralisation (legend).

To further probe the origin of the new 1730 cm^{-1} band the area fraction for this band (AR_{1730}) with respect to both this band and the band at 1699 cm^{-1} (due to dimeric RCOOH) was plotted as a function of α_{nom} (See Fig. S3). Interestingly, the initial AR_{1730} values for the polyacid films (α_{nom} = 0%) were about 0.25 – 0.27, which agrees with the nominal mole fraction of 0.27 for AN present in the nanoparticles with respect to AN and Bd. The AR_{1730} value increased with increasing α_{nom} for both NC50(0.5)S(1) and NS100(1). The increase of AR_{1730} with α_{nom} implies that neutralisation was less facile for RCOOH hydrogen bonded to nitrile groups. We speculate that because the AN segments were less flexible, they were less effective at facilitating the conformational changes required for ionic bonding of the $RCOO^-$ groups to Zn^{2+}.

AN-containing conventional copolymer films have been reported to contain crystallites of AN segments[22]. Accordingly, we investigated several films using WAXD (Fig. 3). All of the diffractograms showed an amorphous peak at $2\theta = 17.5 - 20^{o}$ (5.1 - 4.5 Å) which covered the range that has been reported for PBd[40] and PAN[41] copolymers. The diffractograms also showed a broad maximum at about $2\theta = 40^{o}$ (2.3 Å) which is indicative of more close-packed polymer segments. Closer examination of the lower angle maxima shows that the maximum position moved to lower values as $W_{AN(Tot)}$ increased (see Table 2). This trend is attributed to the influence of AN on chain packing and is consistent with the presence of copolymerised AN segments. The trend is not due to PAN crystallites because the reported diffractograms of PAN show a sharp maximum at[22, 41, 42] $2\theta = 17^{o}$. A sharp maximum is not present for the diffractograms of the AN-containing systems (Fig. 3). Whilst there is a broad maximum for NS100(1) in Fig. 3(a) at $2\theta = 17.5^{o}$ this is attributed to a scattering from a AN-containing copolymer because this maximum is the most intense that is present. Furthermore, the full width at half maximum height (FWHM) for this peak increased with increasing AN content (Table 2). This increase of the broadness of the peak suggests a perturbation of the structure of PBd-MAA upon inclusion of AN and is attributed to copolymerisation of AN. We conclude that the AN units were well dispersed at a molecular level as PBd-AN-MAA chains due to copolymerisation that occurred during NS100(1) and NC50(0.5)S(1) nanoparticle formation.

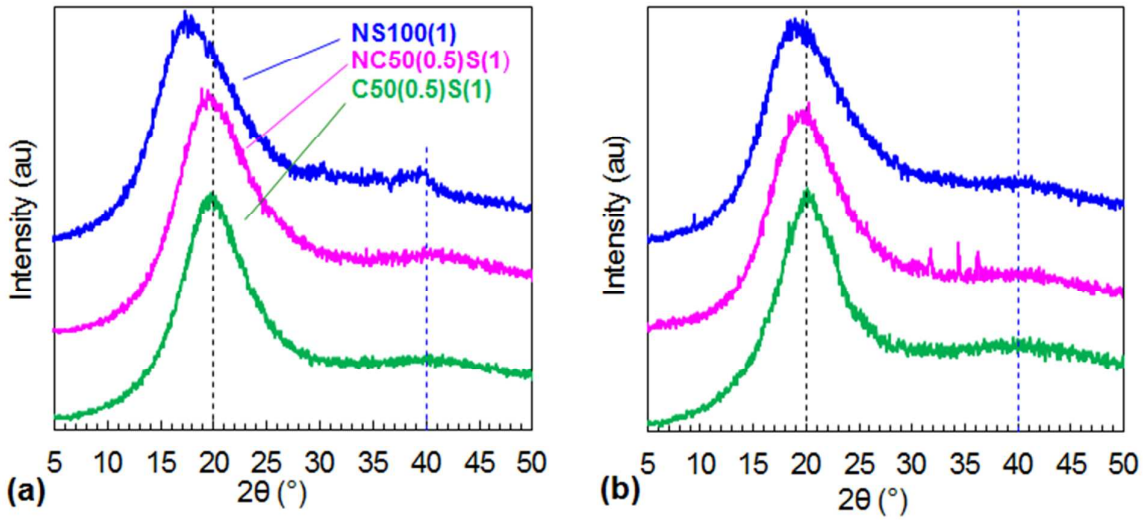

Fig 3. WAXD data for polyacid (α_{nom} = 0, (a)) and neutralised films (α_{nom} = 104 – 117%). The legend applies to both graphs.

Table: 2 Selected data from WAXD measurements.

		0% [b]		~ 100% [b]	
Code	$W_{AN(Tot)}$ [a]	2θ / °	*FWHM* [d]	2θ / °	*FWHM* [d]
NS100S(1)	25.0	17.5	17.8	19.0	17.3
NC50(0.5)S(1)	12.5	19.5	15.6	19.5	15.3
C50(0.5)S(1)	0	20.0	13.2	20.0	13.2

[a] Overall nominal AN concentration (wt.%) in the nanoparticle assuming 100% conversion. [b] Polyacid films. [c] α_{nom} values for the neutralised samples were 104 – 117 %. [d] Full width at half maximum height values from Fig. 3.

The morphology of C50(0.5)S(1) films was studied extensively using AFM in our earlier publications[20, 21]. Here, AFM tapping mode images for the surface of a neutralised NC50(0.5)S(1) film are shown in Fig. 4. Both images show the particulate nature of the surface with many nanoparticles with diameters in the region of about 70 to 100 nm present (inset of Fig. 4(a)). The line profile shows a peak-to-peak height of the order of the diameter of the nanoparticles (Table 1) with a root-mean-square roughness of 27 nm. The surface morphology is in agreement with that expected for a film composed of nanoparticles cast from a nanoparticle dispersion. The surface roughness for the film is relatively low when compared to the film thickness (280 μm).

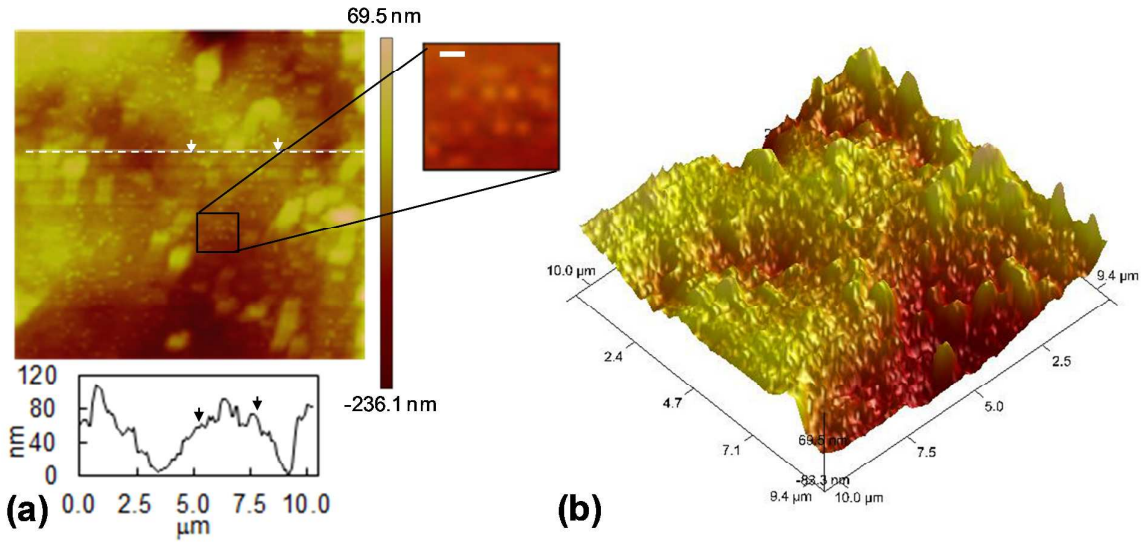

Fig. 4. AFM images and line profile for NC50(0.5)S(1) (α_{nom} = 112%) films. The dimensions of the images in (a) and (b) are 10.5 μm x 10.5 μm. The scale bar for the expanded image from (a) is 200 nm.

Effects of AN on nanostructured film mechanical properties

The temperature-dependent mechanical properties of the films were investigated using DMTA. This technique has proven to be very useful for studying the phase composition of ionomers[43]. We first consider the polyacid films (α_{nom} = 0%) and tanδ (= *E"*/*E'*) vs. temperature data are shown in Fig. 5. (*E"* and *E'* are the loss and storage modulus values, respectively.) Whereas the variable temperature tanδ data for the C50(0.5)S(1) film had only one maximum (-68 ^{o}C), the data for NC50(0.5)S(1) and NC50(4)S(1) had two main maxima. The first maximum at about -70 to -73 ^{o}C is attributed to the T_g of PBd and originated from the core of the nanoparticles. The fact that the -70 ^{o}C peak is absent for the uniform (non-core-shell) NS100(1) film is important because it confirms that this film comprised nanoparticles that contained copolymerised Bd and AN. There was no evidence of phase separated PBd and PAN.

15

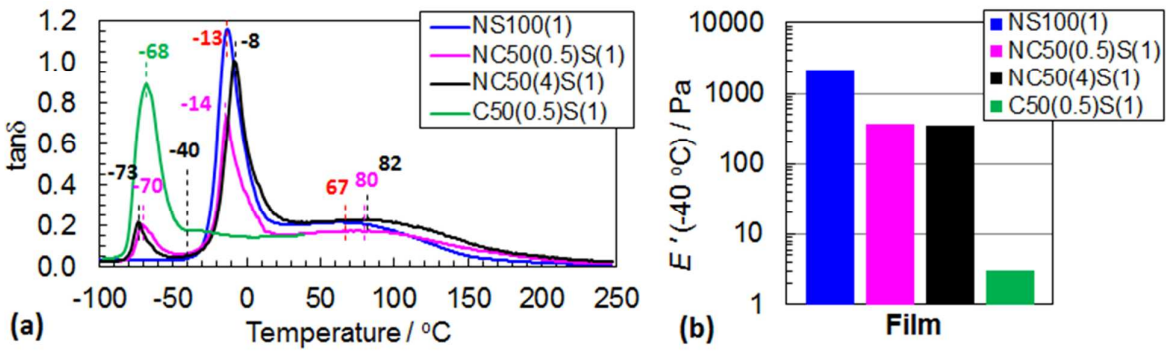

Fig. 5. (a) Temperature-dependence of tanδ for various polyacid films (α_{nom} = 0%). (b) shows the values for *E'* measured at -40 °C.

Compared to the C50(0.5)S(1) films, the AN-containing films contained strong tanδ peaks at -8 to -14 °C (Fig. 5(a)). These peaks are attributed to copolymerised PBd-AN because PAN has a high T_g. (The T_g of PAN has been reported as 105 °C[28].) There are also broad maxima in the region of 67 – 82 °C for the AN-containing systems. (The C50(0.5)S(1) films were too weak at temperatures above 40 °C to allow DMTA data to be measured.) Although the origin of those maxima is not clear, species involving hydrogen-bonded RCOOH groups may have been involved. In summary, there were three phases present for the polyacid AN-containing core-shell systems. Those phases consisted of PBd, PBd-AN and RCOOH-rich species.

The temperature-dependencies of the *E'* data for the polyacid films are shown in Fig. S4. The effects of copolymerised AN on the elasticity of the polyacid films is illustrated from the *E'* values measured at – 40 °C (Fig. 5(b)). The latter temperature is between the T_g for PBd (-68 to -73 °C) and PBd-AN-MAA (-8 to -14 °C). The E'(-40 °C) values decreased in the order: NS100(1) > NC50(0.5)S(1) ~ NC50(4)S(1) > C50(0.5)S(1). This follows the same order as the $W_{AN(Tot)}$ values (Table 1) and shows the importance of AN for increasing film modulus. PAN groups are well known to form physical crosslinks[22] and PAN has a high T_g[28]. The contribution to the *E'* value at -40 °C from the low AN segment mobility due to physical crosslinking increased with $W_{AN(Tot)}$. Room temperature modulus values are considered below using stress-strain data.

The effect of neutralisation on the variable temperature tanδ data was studied (Fig. 6). As α_{nom} increased several major changes occurred. It can be seen that the broad maximum at 50 – 100 °C moved to higher temperatures as α_{nom} increased. It follows that new, lower segment mobility species were created. These species are most likely ionic multiplets and aggregates[7].

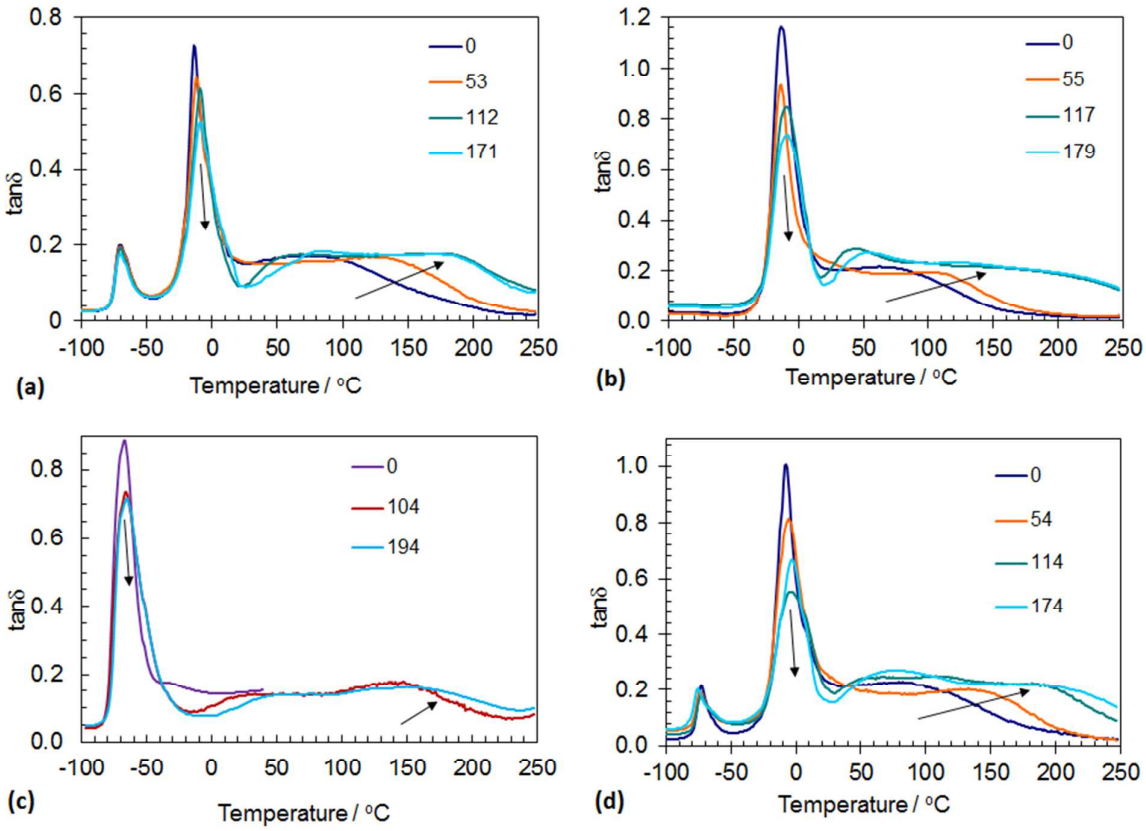

Fig. 6. Effect of temperature on the tanδ data for (a) NC50(0.5)S(1), (b) NS100(1), (c) C50(0.5)S(1) and (d) NC50(4)S(1). The α_{nom} values are shown in the legends.

Fig. 7(a) and (b) show the variations of the T_g and the area for the T_g maxima with α_{nom} due to copolymerised PBd-AN-MAA. The data used are those from Fig. 6(a), (b) and (d) for the tanδ maxima in the temperature region of -14 to -2 °C. The T_g for PBd-AN-MAA increased and the total proportion of the species responsible decreased (as judged by the area under these curves) with increasing α_{nom}. The creation of species (PBd-AN-MAA) through neutralisation with higher T_g and a concurrent decrease of their proportion are signatures of multiplet and cluster formation[44]. The T_g increase is most likely due to restricted chain mobility caused by ionic crosslinking.

17

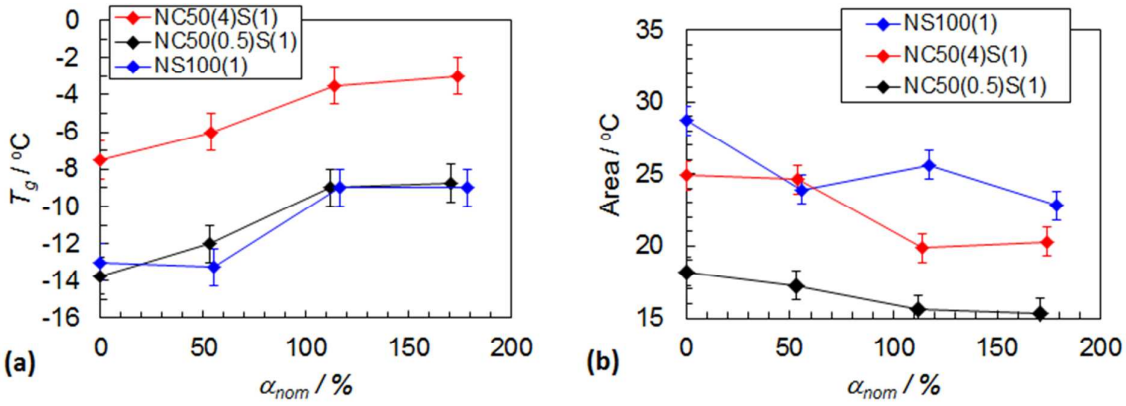

Fig. 7. (a) shows the effect of neutralisation on the T_g due to PBd-AN-MAA. (b) shows the variation of the area of the peak responsible for the T_g in (a) with neutralisation.

Stress-strain data were obtained for the polyacid films at 25 °C (Fig. 8). The data (Fig. 8(a)) show yielding for all films except NC50(4)S(1). The latter film showed extensive plastic flow followed by strain hardening. It can be seen from Fig. 8(a) that the effect of copolymerising AN within NC50(0.5)S(1) films was to increase the stress at a given extension ratio (λ), which is attributed to dipolar interactions between C≡N groups.

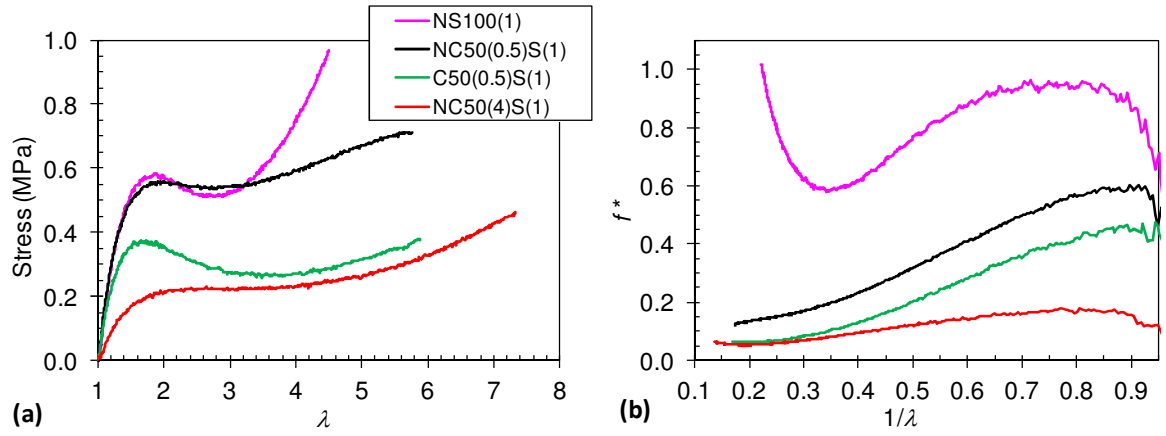

Fig. 8. (a) Tensile stress as a function of extension ratio data and (b) variation of reduced stress with inverse extension ratio data for polyacid films (α_{nom} = 0%). The legend applies to both (a) and (b). See text.

To further investigate the stress (σ) – λ behaviours, the data from Fig. 8(a) were plotted in terms of reduced stress[45] (f^*) as a function of reciprocal λ in Fig. 8(b).

$$f^* = \frac{\sigma}{\lambda - \lambda^{-2}} \qquad (1)$$

For an ideal network of Gaussian chains f^* is equivalent to the shear modulus and should be independent of λ if the number density of elastically-effective chains remains constant. It is evident from Fig. 8(b) that f^* decreases with increasing λ (i.e., decreasing $1/\lambda$) for all of these system, implying strain-induced rupture of elastically effective chains occurred. There is evidence of an increase in f^* for NS100(1) at the highest λ values. The latter is the only system that did not have a distinct PBd phase. This strain hardening behaviour is attributed to the finite extensibility of the AN-containing network, which extended through the whole of the elastomer.

The effect of neutralisation on the stress-strain behaviours is shown in Fig. 9(a) – (d). Neutralisation removed yielding at low λ, increased the gradient (modulus) at low λ and decreased the extension ratios at break (λ_b). The toughness was estimated from the area under the tensile stress-λ curves and the data are plotted in Fig. S5. Whilst neutralisation increased the toughness for all these nanostructured films compared to the non-neutralised states, this occurred at the expense of λ_b. However, the toughness for all the AN-containing films were higher than the C50(0.5)S(1) films whilst the values for λ_b did not decrease (discussed below).

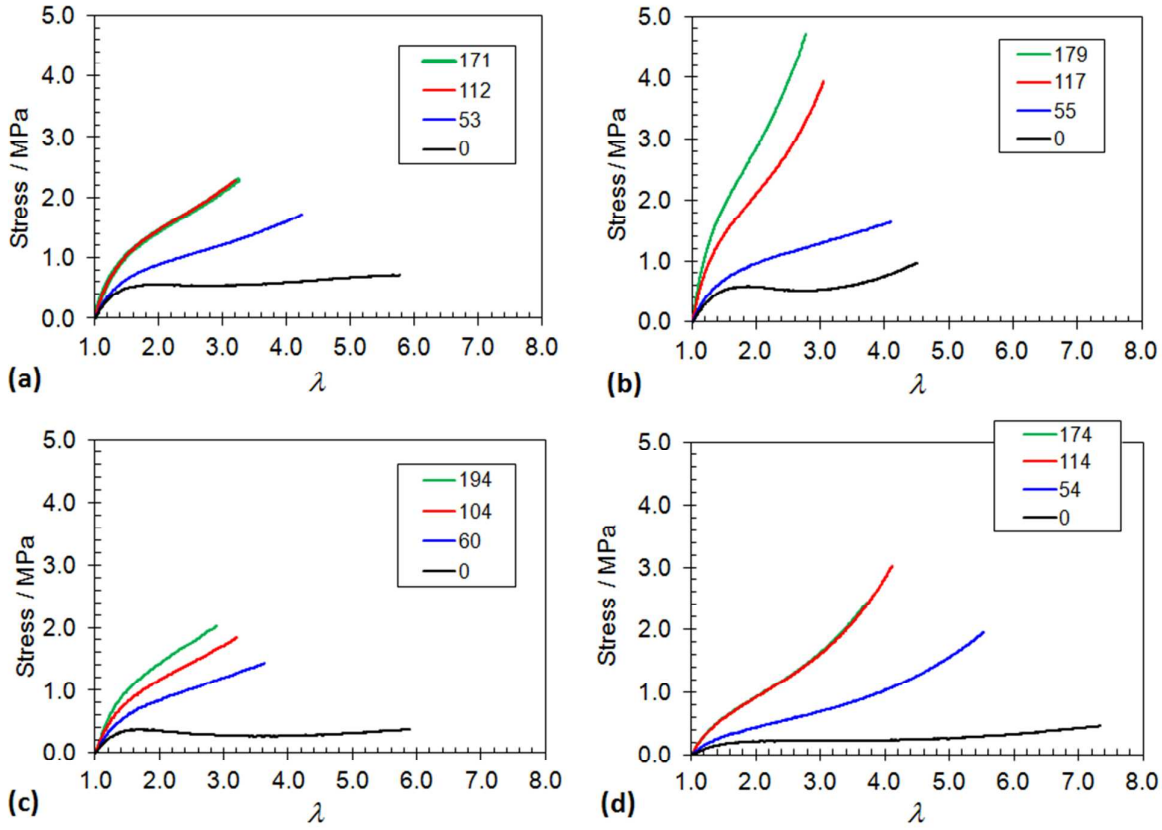

Fig. 9. Tensile stress vs. extension ratio data for (a) NC50(0.5)S(1), (b) NS100(1), (c) C50(0.5)S(1) and (d) NC50(4)S(1). The α_{nom} values are shown in the legends.

Fig. 10(a) and (b) show the effects of neutralisation on the modulus (E) and λ_b for the films. In all cases, E and λ_b increased and decreased, respectively, with increasing α_{nom}. These trends are similar to those reported for neutralisation of poly(ethylene-*co*-MAA) nanocomposites[17]. Interestingly, in the present study it can be seen through comparison of the NC50(0.5)S(1) and C50(0.5)S(1) data that inclusion of AN increased E over the whole neutralisation range (Fig. 10(a)) *without* decreasing λ_b (Fig. 10(b)). The latter important trend shows that physical crosslinks involving AN segments were effective in dissipating energy for the strained films containing AN. This result differs to that observed in the case of neutralisation (Fig. 10 (b)) where λ_b decreased with α_{nom}.

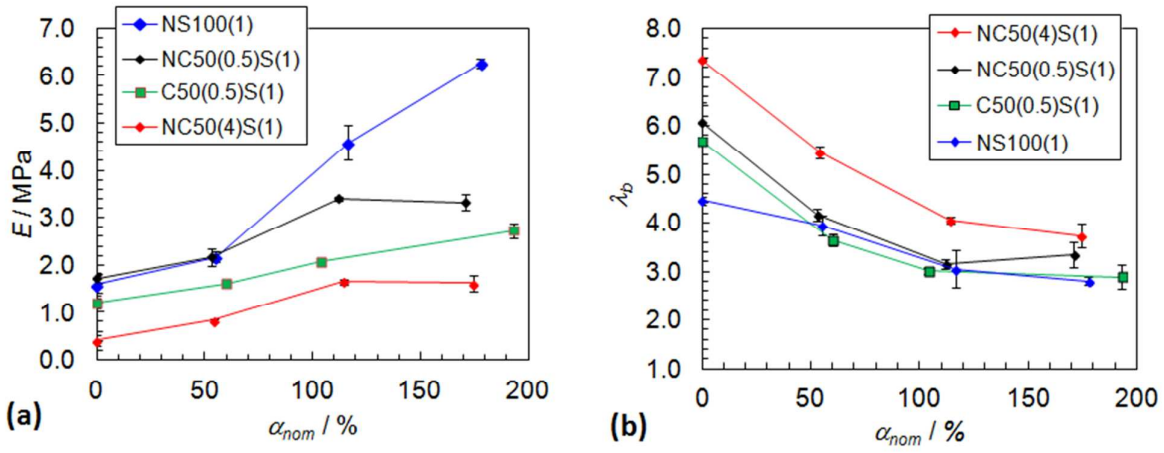

Fig. 10. (a) and (b) show the variation of Young's modulus and the extension ratio at break, respectively, with extent of neutralisation for various films.

The data shown in Fig. 10 for NC50(0.5)S(1) and NS50(4)S(1) also highlight the effect of TDM concentration. Increasing the TDM concentration used for preparing the nanoparticle cores (e.g., 4 wt.% for NC50(4)S(1)) decreased E whilst increasing λ_b. This result is generally in line with the expectation of a decreased number-density of elastically-effective chains through increased branching caused by chain transfer via TDM.

The variation of f^* with $1/\lambda$ for the NC50(0.5)S(1) films at different values for α_{nom} values was also investigated (Fig. S6). Those data show that increasing α_{nom} did not prevent the decrease in crosslinking that occurred with increasing λ (i.e., decreasing $1/\lambda$). Ionic crosslinking was not able to prevent the strain-induced chain scission and / or association scission. Increased α_{nom} did, however, increase f^* at α_{nom} values less than or equal to 112%.

DISCUSSION

The neutralised nanostructured films had three types of crosslinking: (a) conventional covalent crosslinking involving Bd units in the core and shell; (b) physical crosslinking involving AN-segments for the AN-containing systems and (c) physical crosslinks from ionic interactions involving $(Zn^{2+})(RCOO^-)_2$ in the neutralised films. The crosslinking was able to be varied for these nanoparticles in three (experimentally independent) ways. The core-shell nanoparticles enabled use

of TDM to vary the covalent crosslink density of the nanoparticle cores. ZnO was added to neutralise the RCOOH groups in the shell and form ionic crosslinks (ionomers). AN was copolymerised within the shells to provide non-ionic physical crosslinks.

The AN-containing nanostructured films studied in this work showed major structural and property differences compared to the C50(0.5)S(1) systems even though the $W_{AN(Tot)}$ values were modest (12.5 to 25 wt.%). The polyacid AN-containing films showed evidence of a distinct H-bonding environment that was postulated as COOH···N≡C. The RCOOH groups in this environment were less susceptible to neutralisation from added Zn^{2+}. However, once high α_{nom} values were reached in neutralised films the two distinct RCOOH environments were replaced by one common tetrahedral $(Zn^{2+})(RCOO^{-})_2$ environment. This ionic crosslinking unit is consistent with multiplet and cluster species within ionomers[38].

The AN-containing nanostructured films had distinctly different T_g values (and hence compositions) compared to C50(0.5)S(1) as judged by the variable-temperature DMTA data (Fig. 6). There were three distinct T_gs for NC50(0.5)S(1) and NC50(4)S(1) films. Because the WAXD data (Fig. 3) showed that PAN crystallites were not present it follows that AN was approximately uniformly distributed throughout the PBd-AN-MAA chains that comprised the shells of the nanoparticles within the films. A result of incorporating the PAN phase was to increase the T_g values to close to 0 ^{o}C. The decreased segment mobility was due to physical crosslinks that originated from AN segments. The latter caused a major increase of the E' values at -40 ^{o}C compared to C50(0.5)S(1) (Fig. 5(b)).

The E values from stress-λ measurements showed that AN provided a major contribution and this was attributed to the additional physical crosslinks due to AN segments. It is important that λ_B did not decrease when AN was included (Fig. 10(b)). This result suggest that AN behaved as a reversible crosslinker and was very different to the ionic crosslinks (that originated from

neutralisation) which tended to decrease λ_B. Thus, ionic crosslinking and physical crosslinking due to AN had distinctly different physical property outcomes. These differences may relate to the fact that ionic $(Zn^{2+})(RCOO^-)_2$ species involve three units (one Zn^{2+} ion and two $RCOO^-$ groups) that are not able to rapidly rearrange; whereas, AN-based physical crosslinks originate from two C≡N groups[25, 26] and are more able to reform in a new position once disrupted by strain.

Can additional crosslinking due to AN and ionic crosslinking be quantified? To do this we first considered AN crosslinking by comparing the E values for the polyacid NC50(0.5)S(1) and C50(0.5)S(1) films. The number density of elastically-effective chains (ν_e) was estimated using[46]:

$$E = 3\upsilon_e kT \quad (2)$$

This equation assumes an isotropic, ideal, elastic solid with a Poisson ratio of 0.5. Fig. S7(a) depicts a structural model and equations (with derivations) are given in the ESI that allow this question to be addressed. The analysis presented shows that inclusion of AN is equivalent to a change of ν_e in the shells of the nanoparticles ($\Delta\nu_{e(Shell(AN))}$) equal to 8.6 x 10^{25} m^{-3}. From the nominal compositions of the films (Table 1), the number-density of AN groups (C_{AN}) in the NC50(0.5)S(1) shell can be estimated as 2.8 x 10^{27} m^{-3}. Therefore, there were on average 33 AN units (= C_{AN} / $\Delta\nu_{e(S(AN))}$) for every additional elastically-effective chain in the shells of the NC50(0.5)S(1) films compared to C50(0.5)S(1). The AN units were relatively inefficient in creating elastically effective chains. This could be due to low energy involved the intermolecular interactions involving PAN, i.e., dipole-induced dipole attraction[25, 26]. It is the accumulation of many of these interactions along the chains (involving 33 AN units) that provides an elastically effective chain.

A similar approach to that described above was used to estimate the number of ionic $RCOO^-$ groups required for each new elastically effective chain created upon neutralisation of NC50(0.5)S(1) to α_{nom} = 112%. (See ESI.) The analysis presented shows that inclusion of ionically crosslinked

$RCOO^-$ groups was equal to a change in the number-density of elastically-effective chains in the shell ($\Delta\nu_{e(Shell(Neut))}$) of 2.7 x 10^{26} m^{-3}. From the composition of the nanoparticles (Table 1), the number-density of MAA groups (C_{MAA}) in the NC50(0.5)S(1) shell (α_{nom} = 112%) can be estimated as 4.6 x 10^{26} m^{-3}. Therefore, there were on average 1.7 $RCOO^-$ units (= C_{MAA} / $\Delta\nu_{e(S(Neut))}$) for every additional elastically-effective chain in the shells of the NC50(0.5)S(1) films (for α_{nom} = 112%) compared to the polyacid form. A similar analysis to that described above was also conducted for the NC50(4)S(1) and C50(0.5)S(1) films. Those systems had calculated values for the ratio of $RCOO^-$ to new elastically-effective chains in the shells (= C_{MAA} / $\Delta\nu_{e(S(Neut))}$) of 2.1 and 2.9, respectively.

Assuming tetrahedral crosslinking with two $RCOO^-$ groups per Zn^{2+} ion there should be tetra-functional crosslinks within the films at full neutralisation. Generally, a tetrafunctional crosslink will provide two elastically-effective chains[47]. Each $(Zn^{2+})(RCOO^-)_2$ crosslink junction (which should act a tetrafunctional crosslink) should use 2 $RCOO^-$ groups and there should, therefore, be one $RCOO^-$ group per elastically-effective chain. The calculated values of 1.7 and 2.1 (above) are significantly higher than unity. This can be explained by aggregation of the ionic crosslinks within multiplets and clusters[44] as well as inelastic loop formation. In addition, incomplete neutralisation (actual neutralisation being less than α_{nom}) may also contribute to C_{MAA} / $\Delta\nu_{e,S(Neut)}$ values greater than 1.0. Nevertheless, our analysis shows that ionic bonds are much more effective at contributing elastically-effective chains than the reversible interactions involving C≡N (above).

Based on all the data a morphology model for the NC50(0.5)S(1) films is suggested and is depicted in Fig. 11. The AN-containing films benefit from modulus enhancements from both the attractive interactions between AN segments as well as ionomer formation. The reversible nature of the attractive AN-segment interactions meant the ductility was not sacrificed as part of the modulus increase. Nearby AN units provide dipole-dipole attraction via the C≡N groups[25, 26] which provided

reversible physical crosslinks. The $RCOO^-$ groups were more efficient at enhancing ν_e due to their formation of stronger ionic bonds.

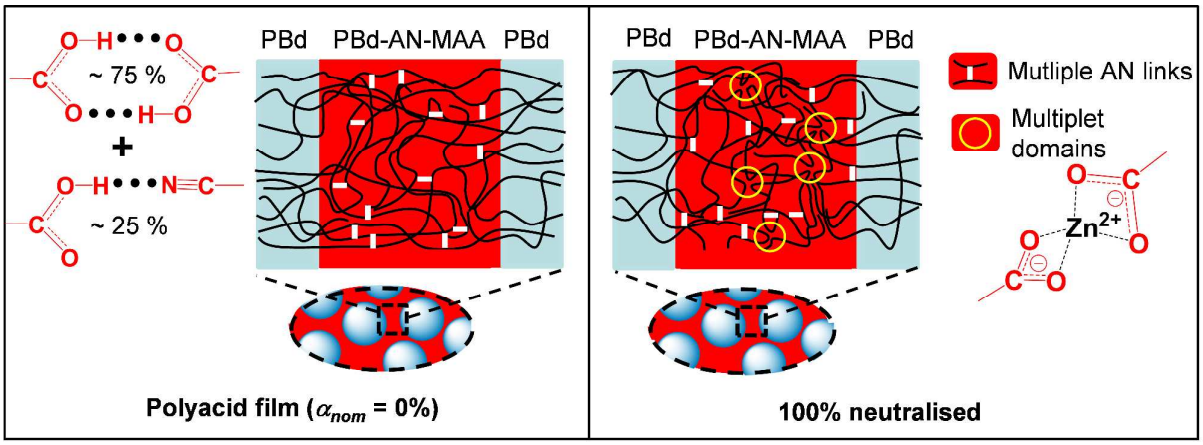

Fig. 11. Depiction of the proposed structure within NC50(0.5)S(1) nanostructured films at different. The white lines represent regions of attractive dipole-dipole interactions between neighbouring C≡N groups which contribute physical crosslinks. The yellow circles represent ionic crosslinks in the form of multiplets.

CONCLUSIONS

This study has examined the structure and properties of AN-containing nanostructured films. Our nanostructured films had three types of crosslinking present: covalent, ionic and physical. The inclusion of AN provided physical crosslinking that had a favourable effect on the mechanical properties, especially the toughness. New FTIR bands found were found for the polyacid films and ascribed to RCOOH···N≡C H-bonding. Inclusion of AN increased modulus significantly but did not decrease λ_b. This is an important outcome because it has potentially wider implications for mechanical property improvements for other nanostructured elastomers and possibly hydrogels. Our analysis indicates that 33 AN shell units produces one additional elastically effective chain. Furthermore, between about 1.5 to 2 ionised $RCOO^-$ groups were required to generate each elastically-effective chain for the neutralised AN-containing films. It follows that the ionic crosslinks were about 10 times more efficient at generating elastically-effective chains than physical crosslinks involving C≡N groups on a per-molecule basis. On the other hand, variation of covalent crosslinking for the core nanoparticles by means of TDM concentration used during core preparation was also an effective means for increasing the ductility. It follows that nanostructured

films based on core-shell nanoparticles provide a very versatile platform for compartmentalising these crosslinking effects and tuning the structure and mechanical properties of ionomers. These new nanostructured ionomers offer the potential to independently tune structure and mechanical properties with versatility that is not available to conventional ionomers.

Acknowledgements

The authors gratefully acknowledge the Royal Thai Government, the Malaysian Government Agency (MARA) and Synthomer Ltd., UK for funding this work. We would also like to thank Dr Bob Groves for his assistance with preparing the nanoparticles.

References

1. J. Borovicka, W. J. Metheringham, L. A. Madden, C. D. Walton, S. D. Stoyanov, and V. N. Paunov. *J. Amer. Chem. Soc.* 2013, **135**, 5282.
2. M. D. Mathew, M. S. Manga, T. N. Hunter, O. J. Cayre, and S. Biggs. *Langmuir* 2012, **28**, 5085.
3. V. J. Mohanraj, T. J. Barnes, and C. A. Prestidge. *Int. J. Pharmaceut.* 2010, **392**, 285.
4. Y. Zheng, W. Turner, M. M. Zong, D. J. Irvine, S. M. Howdle, and K. J. Thurecht. *Macromolecules* 2011, **44**, 1347.
5. J. H. Fendler, and F. C. Meldrum. *Adv. Mater.* 1995, **7**, 607.
6. B. P. Grady. *Polym. Eng. Sci.* 2008, **48**, 1029.
7. A. Eisenberg, B. Hird, and R. B. Moore. *Macromolecules* 1990, **23**, 4098.
8. I. Capek. *Adv. Coll. Interf. Sci.* 2005, **118**, 73.
9. N. Asano, K. Miyatake, and M. Watanabe. *Chem. Mater.* 2004, **16**, 2841.
10. J. A. Kerres. *J. Membr. Sci.* 2001, **185**, 3.
11. L. Billon, M. Manguian, V. Pellerin, M. Joubert, O. Eterradossi, and H. Garay. *Macromolecules* 2009, **42**, 345.
12. A. M. Castagna, W. Wang, K. I. Winey, and J. Runt. *Macromolecules* 2011, **44**, 5420.
13. Y. Nakayama, T. Inaba, Y. Toda, R. Tanaka, Z. Cai, T. Shiono, H. Shirahama, and C. Tsutsumi. *J. Polym. Sci. A; Polym. Chem.* 2013, **51**, 4423.
14. A. Seema, and R. Liqun. *Macromolecules* 2009, **42**, 1574.
15. J. Dong, and R. A. Weiss. *Macromolecules* 2011, **44**, 8871.
16. S. J. Kalista, J. R. Pflug, and R. J. Varley. *Polym. Chem.* 2013, **4**, 4910.
17. L. Cui, C. Troeltzsch, P. J. Yoon, and D. R. Paul. *Macromolecules* 2009, **42**, 2599.
18. A. Ozvald, J. S. Parent, and R. A. Whitney. *J. Polym. Sci. A; Polym. Chem.* 2013, **51**, 2438.
19. M. E. Seitz, C. D. Chan, K. L. Opper, T. W. Baughman, K. B. Wagener, and K. I. Winey. *J. Amer. Chem. Soc.* 2010, **132**, 8165.
20. O. Pinprayoon, R. Groves, P. A. Lovell, S. Tungchaiwattana, and B. R. Saunders. *Soft Matter* 2011, **7**, 247.
21. S. Tungchaiwattana, R. Groves, P. A. Lovell, O. Pinprayoon, and B. R. Saunders. *J. Mater. Chem.* 2012, **22**, 5840.
22. D. Godshall, P. Rangarajan, D. G. Baird, G. L. Wilkes, V. A. Bhanu, and J. E. McGrath. *Polymer* 2003, **44**, 4221.
23. D. Sawai, Y. Fujii, and T. Kanamoto. *Polymer* 2006, **47**, 4445.
24. W. R. Krigbaum, and N. Tokita. *J. Polym. Sci.* 1960, **43**, 467.
25. N. Grassie, and J. N. Hay. *J. Polym. Sci.* 1962, **56**, 189.

26. Y. Nisho, S. Roy, and R. St John Manley. *Polymer* 1987, **28**, 1385.
27. J. Kumamaru, T. Kajiyama, and M. Takayanagi. *J. Cryst. Growth* 1980, **48**, 202.
28. B. Dufour, C. Tang, K. Koynov, Y. Zhang, T. Pakula, and K. Matyjaszewski. *Macromolecules* 2008, **41**, 2451.
29. J. Seuring, and S. Agarwal. *Macromolecules* 2012, **45**, 3910.
30. J.-S. Kim, G. Wu, and A. Eisenberg. Viscoelastic properties of poly(styrene-co-acrylate) and poly(vinylcyclohexane-co-acrylate) ionomers, *Macromolecules* 1994, **27**, 814.
31. C. T. Meyer, and M. Pineri. *Polymer* 1976, **17**, 382.
32. O. Pinprayoon, R. Groves, and B. R. Saunders. *J. Coll. Interf. Sci.* 2008, **321**, 315.
33. M. M. Coleman, and R. J. Petcavich. *J. Polym. Sci.; Polym. Phys.* 1978, **16**, 831.
34. B. Qiao, X. Zhao, D. Yue, L. Zhang, and S. Wu. *J. Mater. Chem.* 2012, **22**, 12339.
35. B. A. Brozoski, P. C. Painter, and M. M. Coleman. *Macromolecules* 1984, **8**, 1591.
36. U. K. Mandal. *Polym. Int.* 2000, **49**, 1653.
37. J. Y. Lee, P. C. Painter, and M. M. Coleman. *Macromolecules* 1988, **21**, 346.
38. P. Antony, S. Bandyopadhyay, and S. K. De. *Polymer* 2000, **41**, 787.
39. L. Ibarra, Alzorriz, M. *J. Appl. Polym. Sci.* 2002, **84**, 605.
40. K. Saijo, Y.-P. Zhu, T. Hashimoto, A. Wasiak, and N. Brzostowski. *J. Appl. Polym. Sci.* 2007, **105**, 137.
41. N. Naraghi, S. N. Arshad, and I. Chasiotis. *Polymer* 2011, **52**, 1612.
42. M. Minagawa, T. Taira, Y. Yabuta, K. Nozaki, and F. Yoshi. *Macromolecules* 2001, **34**, 3679.
43. B. Hird, and A. Eisenberg. *J. Polym. Sci. B; Polym. Phys.* 1990, **28**, 1665.
44. A. Eisenberg. Clustering of ions in organic polymers. A theoretical approach, *Macromolecules* 1970, **3**, 147-154.
45. K. Mayumi, A. Marcellan, G. Ducouret, C. Creton, and T. Narita. *ACS Macro Lett* 2013, **2**, 1065.
46. L. R. G. Treloar. *The physics of rubber elasticity, Oxford Univ. Press, 3rd Ed, Oxford* 2005.
47. P. J. Flory. *Principles of Polymer Chemistry, Ithaca, N. Y.* 1953.